Zoomorphology
https://doi.org/10.1007/s00435-022-00586-0

METHODS PAPERS

Simulating cookiecutter shark bites with a 3D-printed jaw-dental model

Mark A. Grace[1] · Daniel Huber[2] · Kevin Travis[2] · Michael H. Doosey[3] · Jonathan Ford[4] · Summer Decker[4] · Justin Mann[5]

Received: 9 May 2022 / Revised: 5 December 2022 / Accepted: 21 December 2022

Abstract
Ectoparasitic cookiecutter sharks (Chondrichthyes: Squaliformes: Dalatiidae; *Isistius*) share common features for jaw and teeth structure, in particular, robust lower jaws and dignathic heterodonty (upper teeth crowns are more slender and shorter than the broader and longer lower teeth crowns). The jaws and teeth are well suited for feeding by excising a nearly symmetrical oval-flesh bite plug from a variety of prey species including marine mammals, fishes, and squids. There is considerable speculation regarding cookiecutter shark bite dynamics given that natural feeding behavior has not been observed. To elucidate cookiecutter shark bite dynamics, bites were experimentally simulated for the two cookiecutter shark species; the Cookiecutter Shark, *Isistius brasiliensis* (Quoy JRC, Gaimard, P (1824) Zoologie (3) Imprimerie royale) and the Largetooth Cookiecutter Shark, *Isistius plutodus* (Garrick JAF, Springer S (1964) Isistius plutodus, a new squaloid shark from the Gulf of Mexico. Copeia 678–682), using three-dimensional printed models of jaws with teeth. Bite simulations were conducted at standardized jaw bite-gape angles and ballistic gelatin was used to approximate prey flesh, from which aspect ratio analysis of bite wound geometrics was used to determine bite wound morphometrics for each species. The simulated bite experiment also was useful for assessing factors that potentially affect cookiecutter shark total length estimates when based on natural bite geometrics. In addition, the mechanics of producing experimental bites provide new insights related to the necessity for cookiecutter sharks to rotate their body to create nearly symmetrical oval bite wounds.

Keywords Squaliformes · Dalatiidae · *Isistius* spp · Feeding wound morphometrics · Feeding ecology · Forensic zoology

Introduction

The feeding mechanisms of elasmobranch fishes (sharks, skates, rays) exhibit considerable morphological and behavioral diversity, despite having relatively low taxonomic diversity (Huber and Motta 2004). Among elasmobranchs, the ectoparasitic cookiecutter sharks (*Isistius* spp.) and their relatives in family Dalatiidae (dalatiids) remain a persistent enigma owing to their distinct feeding morphology and behaviors (Shirai and Nakaya 1992), and more generally to the experimental intractability of deep-sea elasmobranchs. Cookiecutter sharks have a unique jaw morphology consisting of a robust semicircular scoop-shaped lower jaw (Meckel's cartilage) with a fused symphysis. The considerably reduced upper jaw (palatoquadrate cartilage) is divided into articulated anterior and posterior sections allowing the anterior section to warp dorsally (articulate upward) for tooth attachment onto the surface of prey (Shirai and Nakaya 1992). In addition, a row of serially fused lanceolate teeth on the lower jaw creates a singular blade (Underwood et al. 2016; de Figueiredo and de Carvalho 2018) for cutting into prey after attachment (Shirai and Nakaya 1992). Upper teeth differ from lower teeth (dignathic heterodonty) in that the upper teeth are relatively narrow pointed teeth that do not create a singular blade. During feeding, fleshy labial folds create a seal against prey (Jones 1971) and the enlarged, blade-like teeth of the lower jaw are inserted. Subsequent

✉ Mark A. Grace
Mark.A.Grace@noaa.gov

1 NOAA/NMFS/SEFSC Mississippi Laboratories, Pascagoula, MS, USA

2 University of Tampa, Tampa, FL, USA

3 University of New Orleans, New Orleans, LA, USA

4 University of South Florida Morsani College of Medicine, Tampa, FL, USA

5 Tulane University, New Orleans, LA, USA

Published online: 08 February 2023

lower jaw adduction engages the teeth into the prey resulting in removal of a plug of prey flesh (Shirai and Nakaya 1992).

Bite wound morphometrics and feeding ecology are cookiecutter sharks' attributes that are notably intriguing. The characteristic bite wounds on cetaceans and fishes (Fig. 1 and SI 1) caused by cookiecutter shark feeding behavior range from incomplete dermal abrasions to deep subdermal scoops of missing flesh with relatively smooth oval to round peripheries (Jones 1971; Shirai and Nakaya 1992) and have been used to establish geographic distributions of both cookiecutter sharks and their prey (Muñoz-Chápuli et al. 1988; Goto et al. 2009). Bite wounds on prey that are unique in their geometry and location are useful for distinguishing specific cookiecutter shark prey individuals through repeated observations (Muñoz-Chápuli et al. 1988; Dwyer and Visser 2011; Best and Photopoulou 2016). Bite wound morphometrics related to cookiecutter shark total lengths have been used to examine cookiecutter shark biogeography and feeding strategies (Castro et al. 2018). Stable isotope analysis of cookiecutter shark tissue samples confirms that cookiecutter sharks' prey includes relatively high trophic level fauna (Grace et al. 2018), and cookiecutter sharks can have ontogenetic dietary shifts (Carlisle et al. 2021). However, cookiecutter shark bite wounds are frequently used to simply identify the presence of cookiecutter sharks in general without attempting to distinguish cookiecutter shark species from each other (*I. brasiliensis* or *I. plutodus*) based on bite geometrics or bite morphometrics, or from their dalatiid relatives, some of which have similar teeth and jaws (Ebert et al. 2013).

The objectives of this study were the following: (1) To create three-dimensional (3D) models of the feeding mechanisms of *I. brasiliensis* and *I. plutodus* based on computed tomography (CT) scans, (2) to design and conduct a simulated bite experiment to assess changes in cookiecutter shark bite morphology and bite mass at differing bite gape angles, (3) to evaluate the experimental bite results to identify factors that potentially affect cookiecutter shark total length estimates when based on natural bite wound or natural bite plug geometrics, (4) to test if it is necessary for cookiecutter sharks to rotate their bodies during bite events in order to create the nearly symmetrical oval bite wounds, (5) and use aspect ratio morphometric analysis of experimental bite geometrics to attribute bites to species.

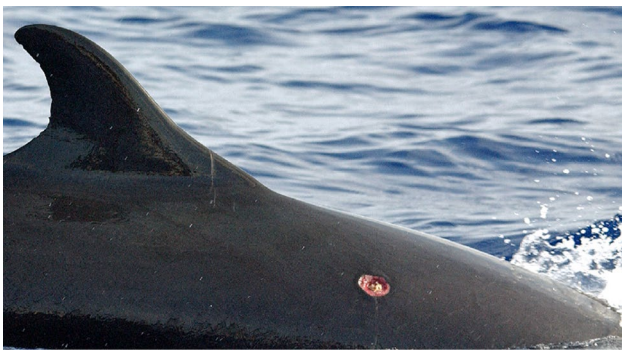

Fig. 1 Dalatiid shark bite wound (pale oval anterior of dorsal fin) on a False Killer Whale (*Pseudorca crassidens*); photo credit NOAA/NMFS/SEFSC

Materials and methods

Specimens and constructing the jaw models

Two cookiecutter sharks (*I. brasiliensis*, 372 mm total length (TL), 169.9 g; *I. plutodus*, 313 mm TL, 87.9 g; Fig. 2) were trawl-captured during a visual survey of cetaceans conducted in the Gulf of Mexico through the National Oceanic and Atmospheric Administration/National Marine Fisheries Service/Southeast Fisheries Science Center (NOAA/NMFS/SEFSC) 2010 Sperm Whale Autonomous Prey Study (SWAPS). Midwater trawls were conducted near Sperm Whale (*Physeter macrocephalus*; Linnaeus 1758) sightings to capture potential sperm whale prey (fishes and squids; Grace et al. 2018). Cookiecutter sharks were initially frozen in seawater and later preserved in 20% formalin, then archived in 70% ethanol at the Tulane University Biodiversity Research Institute (TUBRI) Royal D. Suttkus Fish Collection, Belle Chasse, Louisiana (TUBRI catalog numbers TU 204003 *I. plutodus*, TU 204004 *I. brasiliensis*).

Each specimen was CT scanned with a Lightspeed VCT 64 slice scanner (GE, Fairfield, CT, USA) at 0.625 mm slice thickness through Diagnostic Imaging Services at the University of South Florida (USF) Morsani College of Medicine's Department of Radiology in Tampa, FL, and scans are publicly available through www.MorphoSource.org, Duke University. CT scans were conducted approximately 4 years after the specimens were captured. Virtual reconstruction of the upper and lower jaws with teeth (Fig. 2) was performed with Amira 5.2.4 software (FEI, Hillsborough, OR), and surfaces were further optimized for 3D printing with 3-Matic software (Materialise, Leuven, Belgium). The jaw-teeth models (jaw models) were then scaled 3:1 to facilitate easier manipulation for bite simulations, and 3D-printed using a Form 2 printer (Formlabs Inc., Somerville, MA). Jaw model scaling accuracy was confirmed by comparing jaw model geometrics with the corresponding jaw geometrics for the *I. brasiliensis* and *I. plutodus* specimens used for the model. The upper jaws were hinged with nylon bolts to the lower jaws via constructed tabs (10.0 mm height) that extended from the lower jaw portion on the medial aspect of the jaw joint. These tabs abutted a complimentary planar surface created on the medial aspect of the jaw joint of the upper jaw (Fig. 2), allowing unencumbered rotation of the articulated

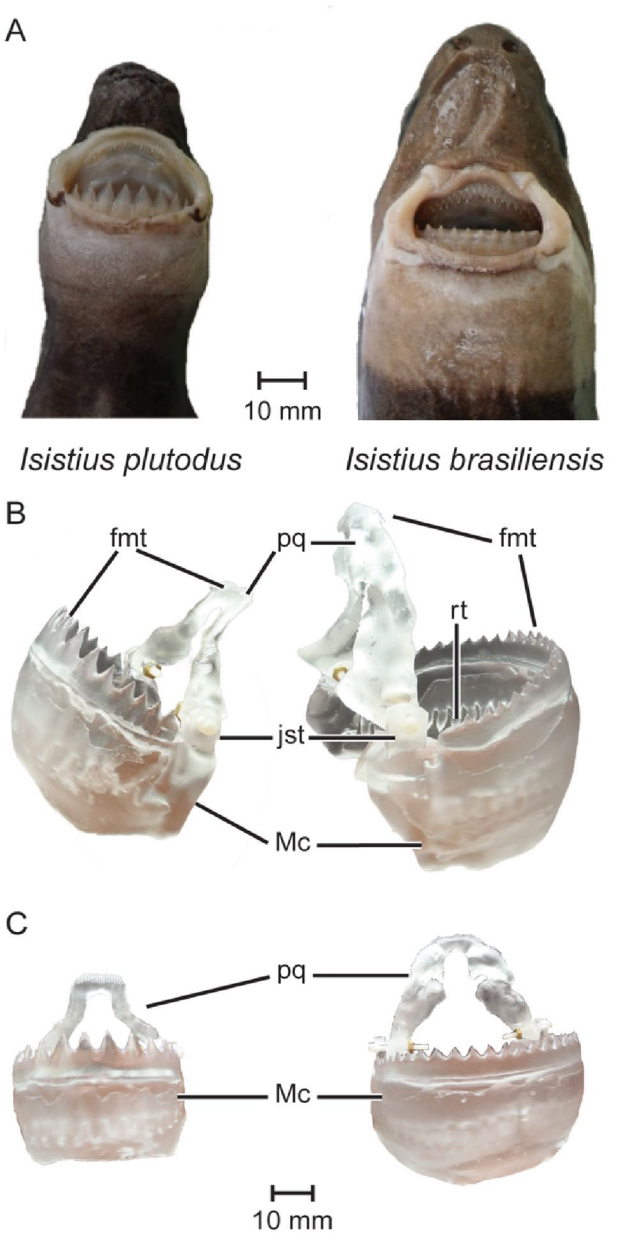

Fig. 2 **A** Venter views of mouth gape for *Isistius plutodus* and *Isistius brasiliensis* (above). **B** and **C**; *Isistius plutodus* left, *Isistius brasiliensis* right 3D-printed jaw models of *Isistius* spp. (3:1); *fmt* functional medial teeth, *pq* palatoquadrate, *rt* replacement teeth, *jst* jaw symphysis tab, *Mc* Meckel's cartilage

lower and upper jaws. The maximum jaw-model bite gape was 150° with further gape restricted by contact between the rear margins of the upper and lower jaws. Components of the feeding mechanism other than teeth and upper and lower jaws (soft tissues, e.g., muscles, ligaments, tendons, labial folds) were not included in the 3D-printed jaw models.

Bite modeling

Ballistic gelatin was used to simulate prey tissue and consisted of 45 g of powdered gelatin dissolved in 1500 ml of 100 °C water (ballistic gelatin density = 1.1 g/ml; volume determined by water displacement). The ballistic gelatin was refrigerated until thoroughly cooled and set (approximately 6 h at 4.0 °C); gelatin could be reused by slightly warming to a liquid state then re-cooling. The process for physically simulating experimental bites was to set the jaws at specific bite gape angles (30°, 60°, 90°, 120° and 150°; wedges were used between the jaw joints to maintain uniform gape) measured via lines extended from the jaw joint to the upper and lower anterior-most medial or symphysial tooth tip and then place the jaws with the anterior mouth opening facing directly down onto the gelatin. The upper jaw center was held fast by hand with minimal pressure to the gelatin surface while the lower jaw was pushed in a forward arc through the gelatin and to closure via a thin metal pushrod lodged in the gap between the lower jaw and the first erupted row of teeth (develop as replacement teeth) on the lingual surface of the jaw (the fused row of erupted teeth orient ventrally; SI 2). To reduce fragmentation of the ballistic gelatin at the periphery of the bite wound and bite plug, uniform bite margins were created by depressing the ballistic gelatin against lower jaw teeth cusps as they broke the ballistic gelatin surface. The characteristic underbite of *I. plutodus* and *I. brasiliensis* enabled lower jaw teeth to completely excise the ballistic gelatin experimental bite plug without twisting or further manipulating the jaw models. Extraneous ballistic gelatin not confined within the lingual surface of lower jaw teeth (mouth cavity) was excluded from the bite plug analysis.

The initial simulated experimental bite (experimental bite) in ballistic gelatin at each bite gape angle established a random bite plug mass (measured to the nearest 1.0 g) that was used as a comparative standard for subsequent experimental bites. Experimental bites were repeated at each bite gape angle until there were two additional experimental bite plugs with masses that varied by less than 15% from the initial simulated bite plug mass standard. The geometrics from the three experimental bites for each bite gape angle were used for morphometric aspect ratio analysis. Even though there was no experimental precedent and any percentage of mass variation between experimental bites at equal bite gape angles could have been used, the 15% metric was established to provide a standardized experimental basis that could be replicated and to maintain a relatively conservative bite comparison standard while still allowing for a limited amount of experimental bite mass and geometric variation.

Experimental bite wound length (L) was measured on the surface of the gelatin from the insertion point of the lower jaw teeth to the point where those teeth emerged from the

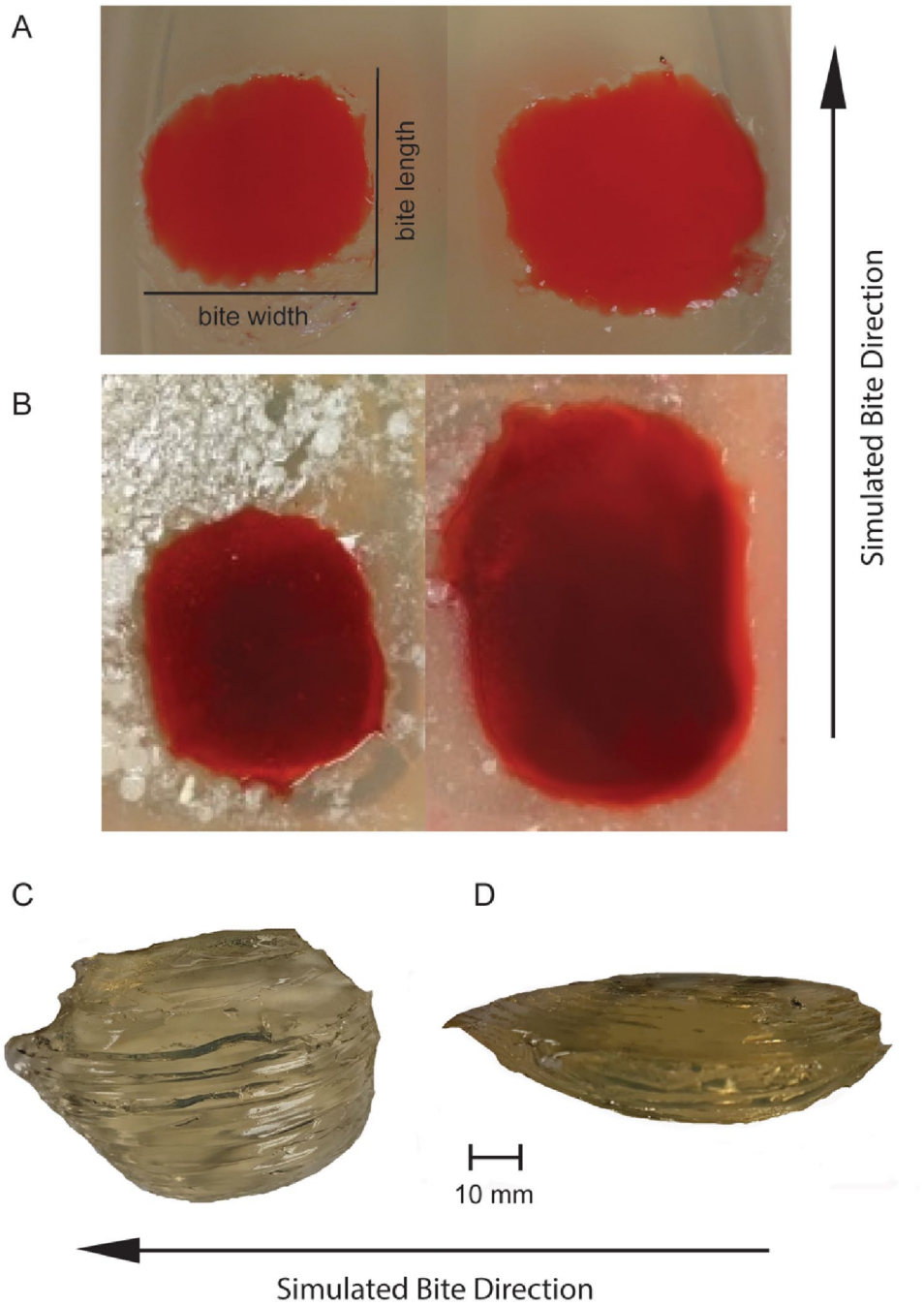

Fig. 3 **A** experimental bite wounds at 60° bite gape angle, *I. plutodus* left, *I. brasiliensis* right, **B** experimental bite wounds at 150° bite gape angle, *I. plutodus* left, *I. brasiliensis* right, **C** *I. brasiliensis* experimental bite plug length at 150° bite gape angle ventral view, **D** experimental bite plug depth at 150° bite gape angle lateral view. Experimental bite wounds were filled with red-dyed water to enhance contrast

gelatin with the excavated bite plug (Fig. 3). Experimental bite wound width (W) was measured on the surface of the gelatin as the distance between the outer-most lateral margins of the excavated region (the maximum diameter of L). Experimental bite wound depth (D) was the measurement of the maximum bite plug depth in lateral view. Experimental bite wound geometrics were reduced in scale by a factor of three to represent each specimen's actual bite geometrics. Experimental bite plug mass was reduced in scale by a factor of 27 to represent each specimen's bite plug mass.

Analysis of experimental bite wounds or bite plug geometrics

Three aspect ratios were calculated to characterize the morphometrics of the excavated experimental bite wounds (L and W) or bite plugs (D). The experimental bite wound length-to-width aspect ratio (LW) corresponds to the coronal plane, while the length-to-depth aspect ratio (LD) corresponds to the sagittal plane, and the width-to-depth aspect ratio (WD) corresponds to the transverse plane. The LW, LD, and WD aspect ratio values were statistically tested to meet the assumptions of a multiple linear regression (homogeneity and normality); the Bartlett test was used for homogeneity between species (Bartlett 1937), and the Shapiro Wilks test for normality within species (Royston 1982). Multiple linear regressions were performed for every aspect ratio measurement by species and bite gape angle to examine experimental bite morphometric differences within and between species. All statistical tests were performed in R statistical program (R Core Team 2016). Bite plug mass expressed as a percentage of specimen mass was compared between species for each bite gape angle, and a regression of bite plug mass as a percentage of specimen mass to bite gape angle also was calculated.

Measurements

Shark jaw and shark jaw model measurements were straight-line measurements taken with dial calipers (SI 2). The lower jaw length was from the center anterior-most medial tooth cusp (*I. brasiliensis*) or the symphysial tooth cusp (*I. plutodus*) to a center point between the last right and left teeth cusps. The lower jaw width measurement was between the last right and left teeth cusps. For both experimental bite wounds and bite plugs, straight-line measurements were taken at the maximum distance for each axis exclusive of ballistic gelatin fragmentation at the periphery. Unlike experimental bite wounds where L was known to be the bite direction (the path of the lower jaw teeth through the ballistic gelatin) and W was the measurement perpendicular to L, for natural bite wounds or natural bite plugs those measurement conditions were indeterminate. Therefore, natural bite wound or natural bite plug measurements are defined as the major bite axis and the minor bite axis. Lower jaw geometrics as a percentage of total length for the experimental cookiecutter sharks (the *I. brasiliensis* and *I. plutodus* specimens used for jaw models) were used to estimate maximum bite wound lengths and widths for non-experimental cookiecutter sharks. The lower jaw length percentage of total length was doubled to estimate a maximum bite wound length (assumes a natural 180° bite gape is possible). The lower jaw width percentage was not doubled.

Results

Experimental bite wound and plug geometry

Bite geometrics were equal between experimental bite wounds and their corresponding experimental bite plugs. Physical appearance of the crater-like experimental bite wounds created by the jaw models (Fig. 3) were similar to bite wounds attributed to *Isistius* spp. in situ (Jones 1971; Shirai and Nakaya 1992; Murakami et al. 2018). Likewise, physical appearance of experimental bite plugs was similar to bite plugs recovered from *I. brasiliensis* stomachs (e.g., Murakami et al. 2018, and Fig. 3). For both *I. brasiliensis* and *I. plutodus*, experimental bite plug mass, bite plug mean mass standard deviation (SD), and LW increased with increasing bite gape angle, while WD decreased with increasing bite gape angle (Tables 1 and 2, Fig. 4 and SI 3 geometric and mass data). Of the three aspect ratios for each

Table 1 Experimental bite plug mass (g) and bite wound geometry (mm) for *I. brasiliensis* and *I. plutodus*. Linear values/3 to rescale to actual specimen morphometrics and mass g/27 to rescale cubic volumes (jaw and teeth model was 3:1 scale)

	Bite gape angle degrees	Bite plug mean mass and SD	Bite plug mean mass % of body mass (g)	Bite wound mean L and SD	Bite wound mean W and SD	Bite plug mean D and SD
I. brasiliensis TL = 372 mm, body mass 169.9 g	30	1.05 ± 0.06	0.62	17.80 ± 1.80	23.30 ± 1.12	5.01 ± 0.12
	60	1.83 ± 0.11	1.08	25.06 ± 3.34	23.89 ± 2.25	5.99 ± 0.12
	90	3.00 ± 0.13	1.77	26.77 ± 2.19	28.12 ± 1.20	7.29 ± 0.19
	120	4.00 ± 0.22	2.35	31.38 ± 1.14	29.12 ± 0.25	8.11 ± 0.79
	150	7.74 ± 0.21	4.56	36.78 ± 1.75	31.50 ± 0.38	12.52 ± 0.30
I. plutodus TL = 313 mm, body mass 87.9 g	30	0.51 ± 0.02	0.58	15.22 ± 0.69	18.17 ± 0.06	3.39 ± 0.25
	60	0.95 ± 0.04	1.08	18.51 ± 3.18	20.82 ± 0.77	5.23 ± 0.21
	90	1.53 ± 0.08	1.74	21.13 ± 1.38	23.03 ± 0.50	6.78 ± 0.67
	120	2.43 ± 0.09	2.77	27.14 ± 0.97	22.70 ± 0.41	7.87 ± 0.55
	150	3.27 ± 0.25	3.72	29.48 ± 0.95	22.74 ± 0.70	9.14 ± 0.91

Table 2 Multiple linear regression of experimental bite wound length-to-width (LW), length-to-depth (LD), and width-to-depth (WD) aspect ratios between *I. brasiliensis* and *I. plutodus* across all bite gape angles

Species	Bite gape angle degrees	Aspect ratios by gape (mean ± SD)	Aspect ratios by species	Multiple linear regression	
				t-value	*p*-value
LW					
I. brasiliensis	30	0.76 ± 0.06	1.01 ± 0.10	0.519	0.608
	60	1.06 ± 0.24			
	90	0.96 ± 0.12			
	120	1.08 ± 0.03			
	150	1.17 ± 0.06			
I. plutodus	30	0.84 ± 0.06	1.03 ± 0.09		
	60	0.89 ± 0.18			
	90	0.92 ± 0.05			
	120	1.20 ± 0.06			
	150	1.30 ± 0.08			
LD					
I. brasiliensis	30	3.56 ± 0.06	3.65 ± 0.08	0.624	0.539
	60	4.17 ± 0.06			
	90	3.67 ± 0.18			
	120	3.90 ± 0.05			
	150	2.94 ± 0.06			
I. plutodus	30	4.50 ± 0.47	3.58 ± 0.43		
	60	3.56 ± 0.76			
	90	3.15 ± 0.50			
	120	3.46 ± 0.16			
	150	3.24 ± 0.25			
WD					
I. brasiliensis	30	4.66 ± 0.26	3.73 ± 0.24	0.808	0.427
	60	3.98 ± 0.41			
	90	3.85 ± 0.13			
	120	3.62 ± 0.35			
	150	2.52 ± 0.05			
I. plutodus	30	5.36 ± 0.23	3.64 ± 0.26		
	60	3.98 ± 0.08			
	90	3.43 ± 0.43			
	120	2.90 ± 0.25			
	150	2.51 ± 0.32			

Ratios by bite gape angle degrees and species represent mean ± standard deviation, and *p*-values calculated through a multiple linear regression across all bite gape angles between species

bite gape angle, LD had the lowest correlation with increasing bite gape angle for both experimental species (Fig. 4). At all bite gape angles morphometric aspect ratios for LD and WD were consistently higher than those for LW (Table 2). When comparing the linear R^2 regressions between species for LW, LD, WD and bite plug mass as a percentage of body mass, the regressions intersected between 60 and 90° experimental bite gape angles (Figs. 4 and 5).

All morphometric aspect ratio data met the normality assumptions. Experimental bite morphometric aspect ratios were not significantly different between species for any of the mean LW, LD and WD bite comparisons (Table 2; $p > 0.05$). Across all gapes, the mean ± standard deviation (mean ± SD) LW for *I. brasiliensis* (1.01 ± 0.18) and *I. plutodus* (1.03 ± 0.21) indicates for both species the experimental bite wound or bite plug is round or elliptical in the coronal plane. The mean ± SD of LD for *I. brasiliensis* (3.65 ± 0.54) and *I. plutodus* (3.76 ± 0.59) indicates for both species the experimental bite wound or bite plug is elliptical in the sagittal plane with the major bite axis oriented vertically relative to the head. Finally, the mean ± SD of WD for *I. brasiliensis* (3.73 ± 0.76) and *I. plutodus* (3.83 ± 1.09) indicates for both species the experimental bite wound or bite plug is elliptical in the transverse plane with the major bite axis

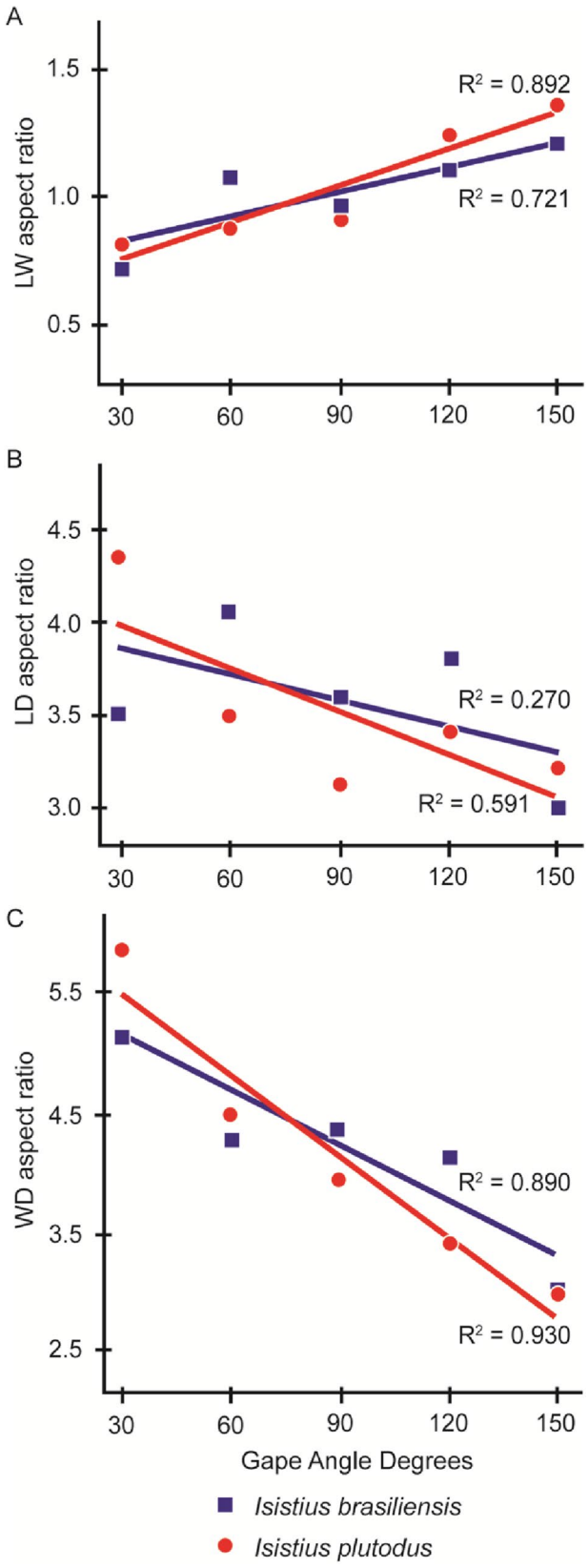

Fig. 4 Experimental bite wound aspect ratios; coronal plane length-to-width (LW) upper, sagittal plane length-to-depth (LD) center, and transverse plane width-to-depth (WD) lower. Data points = mean ± SE; fitted line = mean of predicted values

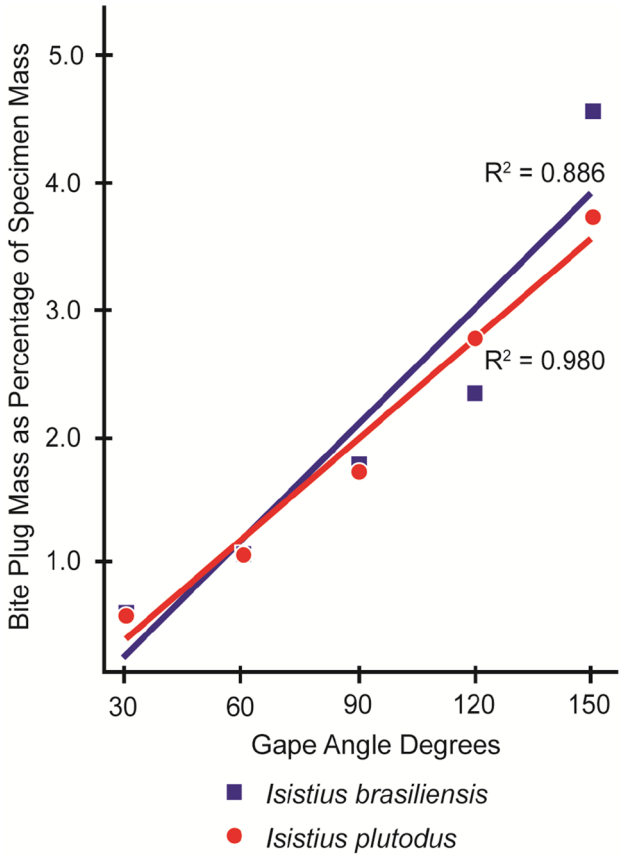

Fig. 5 Linear regressions for experimental mean bite plug mass as a percentage of specimen mass to bite gape angle degrees

oriented laterally relative to the head. For both species, the experimental bite wound or bite plug coronal plane periphery was nearly circular between bite gape angles 30–90°, and more elliptical between bite gape angles 120–150° (Table 1 LW, and Fig. 4). Even though for both species there was a general trend for experimental bite plug mass to increase with bite gape angle (*I. plutodus* $R^2 = 0.9804$; *I. brasiliensis* $R^2 = 0.8859$; Fig. 5), there was variation within species such that experimental bites at equal bite gapes could have unequal bite plug masses or morphometrics (Table 1). This is due to bite-arc differences when conducting replicate experimental bites where a more deeply incised bite differs in mass and dimensions than a more shallow bite. For the experimental *I. plutodus* specimen (313 TL) the estimated maximum bite wound length was 11.0% of the total length, and the maximum bite wound width was 7.0% of the total length. For the experimental *I. brasiliensis* specimen (372 TL) the estimated maximum bite wound length was 10.8% of the total length, and the maximum bite wound width was 7.2% of the total length.

Discussion

Experimental bite morphometric comparison between species

It was not possible to differentiate the experimental bite wounds of the two *Isistius* species based on the analysis of morphometric aspect ratios. Even though there was a minor degree of bite morphometric separation between species the morphometric aspect ratio linear regressions compared between species were very similar for all bite gape angles (Table 2 and Fig. 4). This is possibly due to the morphological similarity of the two species' feeding mechanisms and the variability and overlap of experimental bite morphometrics at various bite gape angles for each species and infrequently between both species, which is a condition that likely occurs in nature. The lack of experimental bite attribution to species by the fundamental morphometric aspect ratio analysis precluded the utility of additional analysis for assessing experimental results. Shape-curvature analysis of jaws has been used for attribution of shark bites to species (Duarte-Neto et al. 2019), but that analysis is problematic for the simulated cookiecutter shark bites because bite morphologies differed between bite gapes (Table 1 and Fig. 3), and for bites that were less than the maximum gape there would be an inconsistent number of reference points needed to fully assess warp. In addition to the simulated bite experiment, other studies support the lack of validity for *I. plutodus* versus *I. brasiliensis* bite attributions to species based on bite wound geometrics (Best and Photopoulou 2016, Feunteun et al. 2018, Niella et al. 2018, Menezes et al. 2022).

The experimental bite simulation was useful for assessing the efficacy of using natural bite wound or bite plug morphometrics as a means to compare, attribute to species, or estimate a cookiecutter shark's total length. An inherent factor that affects the assessments of natural bites is the length of the bite axis that corresponds to jaw width can exceed the length of the bite axis that corresponds to jaw length (e.g., 30–90° Table 1). If assessments of bite wound or bite plug morphometrics do not correctly attribute the source of the major bite axis (whether by jaw length or jaw width), then estimating a cookiecutter shark total length based on those morphometrics potentially is inaccurate (Castro et al. 2018). Additionally, for natural bite wounds and natural bite plugs the cookiecutter shark bite gape angle typically would be unknown and therefore limit the usefulness of applying the experimental bite morphometric aspect ratio results for species attributions.

Feeding ecology, behavior, and physiology

Even though the feeding ecology of cookiecutter sharks is poorly understood in part due to potential prey variability related to diel vertical migrations (Papastamatiou et al. 2010), some feeding behavior aspects can be inferred from the biomechanics of their feeding mechanism (Jones 1971; Shirai and Nakaya 1992). For example, the jaw morphology is uniquely suited for longitudinal twisting (body rotation associated with the bite can be up to a half turn; Shirai and Nakaya 1992) as evidenced by reduced jaw stress and strain energy during rotational biting (Travis et al. 2017; SI 1). However, despite speculation that cookiecutter sharks may rotate their bodies around a central point in order to create and excise the characteristic nearly-oval flesh bite plugs (e.g., Jones 1971), experimental nearly-oval ballistic gelatin bite plugs were created and excised without rotation of the jaws. In addition, upper jaw teeth are irregularly aligned narrow grasping-type teeth that when inserted into prey flesh would inhibit biting action around a central point needed to create a nearly-oval bite wound or bite plug outer margin. Therefore, jaw stabilization and body rotation may be more important for rapid attacks on fast-moving prey during which effective tooth insertion could determine feeding efficacy, or for completely severing prey flesh after the bite is complete. Photographs of incomplete bites demonstrate the inherent difficulties of bite anchoring on highly active prey (e.g., Muñoz-Chápuli et al. 1988; Papastamatiou et al. 2010; Honebrink et al. 2011; Best and Photopoulou 2016).

The scoop-shaped lower jaw and associated sawblade of teeth enables cookiecutter sharks to excise relatively large bite plugs of prey flesh in comparison to their body mass (Table 1). Caloric intake can be determined and compared to metabolic rates by associating the mass of bite plugs consumed with caloric information (Sibly et. al 2012) for specific prey tissue types (e.g., whale blubber 9450 kcal/kg, Brody 1968; squid 800 kcal/kg, Lockyer 1981). A known metabolic rate is important when estimating the frequency with which cookiecutter sharks employ their remarkable feeding method and thereby expose themselves to considerable danger from the much larger and more powerful animals they parasitize (e.g., tunas; Isouchi 1970). The metabolic rate of cookiecutter sharks is unknown but it likely varies depending on prey tissue. However, if the theory of metabolic scaling with respect to body size (Kleiber 1932; Sibly et al. 2012) holds true among sharks then for specific prey tissue digested at equivalent body temperatures (metabolic rates for some elasmobranchs can be affected by endothermy; Carlson et al. 2004) cookiecutter sharks may not need to feed very often compared to larger sharks due to the cookiecutter shark's relatively small size and ability to excise relatively large bite plugs (e.g., 4.6% body mass;

Table 1). For example, the Great White Shark (*Carcharodon carcharias*) can be sustained approximately 1.5 months on a single meal of 3.2% of its body mass (Carey et al. 1982). Comparatively, it is possible that cookiecutter shark feeding events can occur rather infrequently, thereby reducing the risk of injuries or death related to their unique feeding behavior that often entails parasitizing much larger animals that could consume them. For both cookiecutter sharks used for simulating the experimental bites the maximum bite plug mass/body mass (Table 1) was within range of single bite plug mass/body mass for *I. brasiliensis* (0.85–6.72%; Murakami et al. 2018). For an entire *I. brasiliensis* stomach contents with two bite plugs, together they were 14.7% of body mass (Murakami et al. 2018).

Experimental bias

The experimental bite wound periphery could have minor irregularities due to broken edges in the ballistic gelatin (Fig. 3). Another source of experimental bias was the bite depth due to the arc of the downward bite motion of the lower jaw in the ballistic gelatin. Care was taken to assure experimental bite uniformity by not excessively depressing the upper jaw into the ballistic gelatin during the bite simulation. However, the various bite plug masses for each degree category of jaw gape indicates that bite arcs differed (Table 1). Experimental bite plug mean mass was more variable for larger bite gapes compared to smaller bite gapes (Table 1). Bite plug width sometimes slightly exceeded the jaw model's distance between the two rear-most lateral teeth cusps because the Meckel's cartilage lateral margin extended slightly beyond the lower jaw teeth outer margins. Considering soft tissues for joining the upper and lower jaws were not replicated by the 3D-jaw model, bite wound morphometrics and bite plug mass for each jaw-gape degree category may have been affected since the jaw joints of the jaw model may function differently than the jaw joints of live specimens that utilize jaw soft tissues. Soft-tissue mouth features that potentially affect bite biomechanics were also lacking from the jaw models and those features can vary depending on species (de Figueiredo and de Carvalho 2018). Additionally, the maximum gape for experimental jaws (150°) could be less than or greater than the maximum gape for live specimens since the effects of soft tissues (e.g., musculature) on the gape of live specimens are unknown. Even though the specimens were frozen on the day of their capture there may have been a potential bias for jaw morphometric differences between the jaw model and the live specimen jaws related to shrinkage due to freezing and preservation that was not considered for the purposes of constructing the jaw-teeth 3D-model.

The comparisons of the experimental cookiecutter shark bite wound morphometrics and the associated bite plug masses does not account for the possible natural range of potential allometric variations for jaw geometrics as is documented for other elasmobranchs (Huber et al. 2006; Habegger et al. 2012). Squaliformes ontogenic allometric growth was addressed by Garrick (1960) and one of those differences was for head length to be proportionally longer in juveniles compared to their adult size classes. However, potential allometric differences for cookiecutter shark jaw geometrics and their components has not been established except for the increase of *I. brasiliensis* jaw width in proportion to the increase for specimen total length (Muñoz-Chápuli et al. 1988). Relevant to potential allometric differences is the *I. plutodus* was a male (313 mm TL) with calcified claspers indicating sexual maturity (Carrier et al. 2004), and the female *I. brasiliensis* was 372 mm TL that is below the minimum size at maturity (Ebert et al. 2013).

The experimental bite results at the various bite gape angles (Table 1) may approximate some but not all of the variability that naturally occurs considering the numerous possibilities for predator-attack orientation and prey orientation. For both species the experimental 60° bite gape was the minimum gape for the upper jaw teeth cusps to fully anchor in the ballistic gelatin. Considering the upper jaw's anterior palatine plate section can warp dorsally (Shirai and Nakaya 1992) it is possible that bites in nature may have bite gapes less than 60° and still successfully anchor upper teeth; 30° experimental bites were included to address this possibility (Table 1). The bite experiment also does not account for the important effects of cookiecutter sharks' forward momentum, bite velocity, or densities of various prey tissues because only ballistic gelatin was used in bite simulations. Understandably, those variables along with predator and prey behavior potentially affect bite wound configurations. In addition, the ballistic gelatin surface was level so the experimental bites do not account for outer-surface contours of various prey species where bites could occur and that would likely affect natural bite wound or natural bite plug geometrics or mass. Even though there may have been post-bite geometric or mass changes for natural bite plugs (e.g., those reported by Murakami et al. 2018), specifically digestive effects on bite plugs, those changes may not have had much bearing as it relates to the bite experiment. The bite plug mass percentages of body mass for natural bite plugs removed from *I. brasiliensis* stomachs (Murakami et al. 2018) was generally comparable or greater than the mass percentages of experimental bite plugs.

Comparing natural with experimental bite wound or bite plug geometrics is useful for assessing some of the limitations of the experimental cookiecutter shark jaw models for accurately simulating bites. For example, two bite plugs with the longest major bite axis for an *I. brasiliensis* (65 mm) were independently collected by stomach sampling two different specimens with total lengths of 400 mm

(Castro et al. 2018) and 480 mm (Murakami et al. 2018). However, the estimated maximum bite lengths (10.8% of the total length) for those cookiecutter sharks is 43.2 mm and 51.8 mm respectively. One explanation for the discrepancy is the jaw model does not replicate the full range of natural bite biomechanics due in part to the lack of dorsal warping of the articulated anterior palatine plate of the upper jaw. A dorsal warp of the anterior upper jaw can facilitate a bite axis length increase for a natural bite (Shirai and Nakaya 1992) compared to a bite from an equally sized upper jaw that does not warp dorsally (e.g., the 3D-jaw model). Other bite biomechanics that possibly contribute to a bite length increase are the articulations between lower jaw components; ceratohyal and mandibular, mandibular knob and hyomandibula, hyomandibula and ceratohyal, basihyal and ceratohyal (Shirai and Nakaya 1992). Those articulations when distended in the fully open-jaw position would enable the lower jaw to distend ventrally and still allow for proper insertion of lower jaw teeth into prey (Shirai and Nakaya 1992). Therefore, estimates of a specimen's total length based on a lower-jaw length dependent bite axis could be affected by the combination and extent of upper jaw dorsal warping and lower jaw component articulations. As an example, based on the difference between the 400 mm TL *I. brasiliensis* 65 mm bite plug major axis compared to its 43.2 mm estimated maximum bite length, the combination of upper jaw warp and lower jaw component articulations can increase a major bite axis length by 35% (exclusive of prey surface contours). *I. brasiliensis* estimated total lengths based on bite geometrics can be underestimated by 40% or overestimated by 36.5% (Castro et al. 2018) thus, based on the simulated bite experiment, some of those estimated total length differences are due to variable natural bite biomechanics in addition to inaccurate attribution of bite axis L versus W. If the *I. brasiliensis* bite biomechanics hold true for *I. plutodus* that has many comparable jaw components (de Figueiredo and de Carvalho 2018), then *I. plutodus* bite wound or bite plug geometrics similarly would be affected.

Conclusion

In summary, the simulated cookiecutter shark bite experiment was useful for expanding and assessing characterizations of elasmobranch bite dynamics and feeding ecology. CT scan data can be used to create 3D-printed cookiecutter shark jaw models for simulating bite wound configurations that resemble similar configurations of natural bite wounds and natural bite plugs. Within the limits of the experiment there were no statistically significant differences between the *Isistius* spp. bite morphometric aspect ratios when comparing standardized bite gape angles, however, comparisons of bite morphologies and bite mass provided probable sources of morphological and mass variations for natural bites. The extent of the *Isistius* spp. anterior upper jaw dorsal warp and lower jaw component articulations can increase a lower-jaw dependent natural bite length, and that is important when estimating cookiecutter shark total lengths based on bite geometrics or when assessing associated bite plug mass/body mass. While cookiecutter shark predation and metabolic dynamics are largely unknown the experimental bite plug masses as a percentage of specimen mass elucidate possible feeding energetics. Based on the mechanics of producing the experimental bites with the jaw models, cookiecutter sharks do not need to rotate their bodies in order to create or excise nearly symmetrical oval-bite wounds or bite plugs. The simulated cookiecutter shark bite experiment could generate other bite morphometric aspect ratios that are applicable for assessing bites provided there is a full range of cookiecutter shark sizes of each sex used for 3D-jaw modeling, coupled with decreasing or increasing the mass variation between experimental bites at additional standardized jaw gape angles. Additionally, constructing a 3D-jaw model that replicates anterior upper jaw warp and lower jaw component articulations would increase experimental options that are useful for further assessing cookiecutter shark bite biomechanics.

Supplementary Information The online version contains supplementary material available at https://doi.org/10.1007/s00435-022-00586-0.

Acknowledgements The NOAA/NMFS/SEFSC marine mammals/protected species group and the NOAA Ship PISCES facilitated the survey and specimen collections. U.S. Bureau of Energy Management (Interagency Agreement M09PG0014) and NOAA provided survey funding and permitting. HL Bart (TUBRI) coordinated specimen archival and access. The imaging staff of USF Health Radiology Diagnostic Imaging Facility conducted CT scans. JSS Denton (University of Florida) and C Jones (NOAA/NMFS) contributed comments and editing. All experimental methods were conducted in accordance with relevant guidelines and regulations, and were approved by the NOAA/NMFS Southeast Regional Office Committee in St. Petersburg, Florida (Scientific Research Permit No. 779-1633; granting date: 9 January 2009). NOAA/NMFS does not endorse any of the products or software mentioned.

Author contributions Experimental concept MAG and DH. Methodology MAG, DH, KT, MHD. Statistical analyses DH, KT, MHD, MAG. Measurements, weights and photographs MAG, KT. Specimen CT scanning DH, KT, JF, SD, MAG. Scan data preparation, modeling and 3D printing DH, KT, JF, SD. Specimen collection, archiving and accessing JM, MHD, MAG. All authors contributed to the study conception and design and reviewed the final version of the manuscript.

Data availability The authors declare that data supporting the findings of this manuscript are available within the article and its Supplementary information files.

Declarations

Conflict of interest The authors declare that they do not have any conflict of interest.

Nagoya protocol The content of the paper is not affected by the Nagoya Protocol.

References

Bartlett MS (1937) Properties of sufficiency and statistical tests. Proc Royal Soc A 160:268–282

Best PB, Photopoulou T (2016) Identifying the "demon whale-biter": Patterns of scarring on large whales attributed to a cookie-cutter shark *Isistius* sp. PLoS ONE 11(4):e0152643

Brody S (1968) Bioenergetics and Growth. Hafner Pub. Co., New York, p 1023

Carey FG, Gabrielson G, Kanwisher JW, Brazier O, Casey JG, Pratt Jr HL (1982) The white shark, *Carcharodon carcharias*, is warm-bodied. Copeia. 254–260

Carlisle AB, Allan EA, Kim SL, Meyer L, Port J, Scherrer S, O'Sullivan J (2021) Integrating multiple chemical tracers to elucidate the diet and habitat of cookiecutter sharks. Sci Rep 11(1):1–16

Carlson JK, Goldman KJ, Lowe CG (2004) Metabolism, energetic demand, and endothermy. In: Carrier JC, Musick JA, Heithaus MR (eds) Biology of sharks and their relatives. CRC Press, Boca Raton, pp 203–224

Carrier JC, Pratt HL Jr, Castro JL (2004) Reproductive biology of elasmobranchs. In: Carrier JC, Musick JA, Heithaus MR (eds) Biology of sharks and their relatives. CRC Press, Boca Raton, pp 269–285

Castro J, Anllo T, Mejuto J, García B (2018) Ichnology applied to the study of Cookiecutter shark (*Isistius brasiliensis*) biogeography in the Gulf of Guinea. Environ Biol Fishes 101(4):579–588

de Figueiredo Petean F, de Carvalho MR (2018) Comparative morphology and systematics of the cookiecutter sharks genus *Isistius* Gill (1864) (Chrondrichthyes:Squaliformes:Dalatiidae). PLoS ONE 13(8):0201913. https://doi.org/10.1371/journal.pone.0201913

Duarte-Neto P, Rodrigues J, Lessa R (2019) Shape analysis of shark jaws as a tool to identify species involved in incidents with humans. J Forensic Leg Med 64:23–27

Dwyer SL, Visser IN (2011) Cookie cutter shark (*Isistius sp.*) bites on cetaceans, with particular reference to killer whales (Orca) (*Orcinus orca*). Aquat Mamm 37(2):111–138. https://doi.org/10.1578/AM.37.2.2011.111

Ebert DA, Fowler S, Compagno L (2013) Sharks of the world: a fully illustrated guide. Wild Nature Press, Plymouth, NH, USA

Feunteun A, Schrevel C, Verhaegen M, Chevallier D, Duchemin M, Ziani N, Montgolfer B (2018) First evaluation of the cookiecutter-sharks (*Isistius sp.*) predation pattern on different cetacean species in Martinique. Environ Biol Fishes 101(5):749–759. https://doi.org/10.1007/s10641-018-0735-1

Garrick JAF (1960) Studies on New Zealand Elasmobranchii. Part XII. The species of squalus from New Zealand and Australia; and a general account and key to the New Zealand Squaloidea. Trans R Soc NZ 88:519–557

Garrick JAF, Springer S (1964) Isistius plutodus, a new squaloid shark from the Gulf of Mexico. Copeia, pp 678–682

Goto M, Kanda N, Pastene LA, Bando T, Hatanaka H (2009) Differences in cookie cutter shark-induced body scar marks between J and O stocks of common minke whales in the western North Pacific. IWC Scientific Committee, Paper SC/J09/JR28 (9):1–7

Grace MA, Aichinger Dias L, Maze-Foley K, Sinclair C, Mullin KD, Garrison L, Noble L (2018) Cookiecutter shark bite wounds on cetaceans of the Gulf of Mexico. Aquat Mamm 44(5):491–499. https://doi.org/10.1578/AM.44.5.2018.491

Habegger ML, Motta PJ, Huber DR, Dean MN (2012) Feeding biomechanics and theoretical calculations of bite force in bull sharks (*Carcharhinus leucas*) during ontogeny. Zoology 115(6):354–364

Honebrink R, Buch R, Galpin P, Burgess GH (2011) First documented attack on a live human by a cookiecutter shark (Squaliformes, Dalatiidae: *Isistius sp.*). Pac Sci 65(3):365–374. https://doi.org/10.2984/65.3.365

Huber DR, Motta PJ (2004) Comparative analysis of methods for determining bite force in the spiny dogfish *Squalus acanthias*. J Exp Zool 301A:26–37

Huber DR, Weggelaar CL, Motta PJ (2006) Scaling of bite force in the blacktip shark *Carcharhinus limbatus*. Zoology 109:109–119

Isouchi T (1970) A cigar shark, *Isistius brasiliensis* from the tropical water of the eastern Pacific. J Ichthyol 17:124–125

Jones EC (1971) *Isistius brasiliensis*, a squaloid shark, probable cause of crater wounds on fishes and cetaceans. Fish Bull 69(4):791–798

Kleiber M (1932) Body size and metabolism. Hilgardia, J Agric Sci 6(11):315–353

Linnaeus C (1758) Systema Naturae per regna tria naturae, secundum classes, ordines, genera, species, cumcharacteribus, differentiis, synonymis, locis 1(10):1–824

Lockyer C (1981) Growth and energy budgets of large baleen whales from the Southern Hemisphere. FAO Mamm Seas 5(3):502

Menezes R, Marinho JPD, de Mesquita GC, da Silva GB (2022) Cookiecutter shark (*Isistius* spp.) bite patterns on pelagic fishes in aggregated schools in the western equatorial Atlantic Ocean. Environ Biol Fish. https://doi.org/10.1007/s10641-022-01257-1

Muñoz-Chápuli R, Rel Salgado JC, De La Serna JM (1988) Biogeography of *Isistius brasiliensis* in the North-Eastern Atlantic, inferred from crater wounds on Swordfish (*Xiphias gladius*). J Mar Biol Assoc 68:315–321

Murakami C, Yoshida H, Yonezaki S (2018) Cookie-cutter shark *Isistius brasiliensis* eats Bryde's whale *Balaenoptera brydei*. Ichthyol Res 65:398–404. https://doi.org/10.1007/s10228-018-0619-6

Niella Y, Duarte LAG, Bandeira VR, Crespo O, Beare D, Hazin FHV (2018) Cookie-cutter shark *Isistius* spp. predation upon diferent tuna species from the south-western Atlantic Ocean. J Fish Biol 92(4):1082–1089. https://doi.org/10.1111/jfb.13569

Papastamatiou YP, Wetherbee BM, O'Sullivan J, Goodmanlove GD, Lowe CG (2010) Foraging ecology of cookiecutter sharks (*Isistius brasiliensis*) on pelagic fishes in Hawaii, inferred from prey bite wounds. Environ Biol Fish 8:361–368. https://doi.org/10.1007/s10641-010-9649-2

Quoy JRC, Gaimard P (1824) Zoologie (3) Imprimerie royale

R Core Team (2016) R: A language and environment for statistical computing. R Foundation for Statistical Computing, Vienna, Austria. https://www.R-project.org/

Royston P (1982) An extension of Shapiro and Wilk's *W* test for normality to large samples. J Appl Stat 31:115–124

Shirai S, Nakaya K (1992) Functional morphology of feeding apparatus of the cookie-cutter shark, *Isistius brasiliensis* (Elasmobranchii, Dalatiinae). Zool Sci 9(4):811–821

Sibly RM, Brown JH, Kodric-Brown A (2012). Metabolic ecology: a scaling approach. John Wiley & Sons, p 395

Travis K, Grace M, Ford J, Decker S, Huber D (2017) Structural mechanics of cookiecutter shark jaws. Soc. Abstract. Integrative and Comparative Biology, New Orleans

Underwood C, Johanson Z, Smith MM (2016) Cutting blade dentitions in squaliform sharks form by modification of inherited alternate tooth ordering patterns. Royal Soc Open Sci 3(11):160385